Atmos. Chem. Phys. Discuss., 9, 7531–7554, 2009
www.atmos-chem-phys-discuss.net/9/7531/2009/

Atmospheric Chemistry and Physics Discussions

This discussion paper is/has been under review for the journal *Atmospheric Chemistry and Physics (ACP)*. Please refer to the corresponding final paper in *ACP* if available.

Clarification on the generation of absolute and potential vorticity in mesoscale convective vortices

R. J. Conzemius[1,2] **and M. T. Montgomery**[1,3]

[1]Department of Atmospheric Science, Colorado State University, Fort Collins, Colorado, USA
[2]WindLogics, Inc., Grand Rapids, Minnesota, USA
[3]Naval Postgraduate School, Monterey, California, USA

Received: 18 February 2009 – Accepted: 27 February 2009 – Published: 23 March 2009

Correspondence to: R. J. Conzemius (robert.conzemius@att.net)

Published by Copernicus Publications on behalf of the European Geosciences Union.

Abstract

The purpose of this paper is to clarify what we think are several outstanding issues concerning the predominant mechanism of vorticity generation in mesoscale convective vortices (MCVs). Using idealized mesoscale numerical simulations of MCV development, we examine here the vertical vorticity budgets in order to quantify the contributions of flux convergence of absolute vorticity versus tilting in the generation of MCV vorticity. In addition, we examine the corresponding diabatic heating profiles. By partitioning the diabatic heating between convective and stratiform regions, we elucidate the respective roles of convective and stratiform precipitation in the generation of potential vorticity (PV).

The analyses indicate that the horizontal flux convergence of vertical vorticity is the dominant mechanism for the spin-up and intensification of mid-level absolute vorticity. Indeed, diabatic heating and circulation budgets demonstrate that the vertical gradient of diabatic heating is supportive of low- to mid-level PV generation. During the early stages of MCV development, convective precipitation plays the dominant role in the PV generation; later on, the stratiform precipitation expands and becomes a larger contributor, particularly in low-CAPE background environments.

1 Introduction

In their pioneering paper outlining a theory for the maintenance of long-lived mesoscale convective systems (MCS)s, Raymond and Jiang (1990) stated that "the convective and anvil regions have the same qualitative effect on potential vorticity distributions, i.e. potential vorticity in the lower half of the troposphere is increased, whereas potential vorticity near the tropopause is decreased". With regard to the absolute vorticity generation in mesoscale convective vortices (MCVs), it is commonly thought that, because the vortex resides in an area of stratiform precipitation, the stratiform processes must be largely responsible for generating its absolute vorticity (Hertenstein and Schubert,

ACPD

9, 7531–7554, 2009

1991; Johnson and Bartels, 1992; Fritsch et al., 1994; Davis and Trier, 2002).

"This large derivative of the heating, coupled with the longer influence time associated with the width of the stratiform region, allows the potential vorticity signature of the stratiform region to dominate over the signature of the convective line" (Hertenstein and Schubert, 1991).

"Intensification of the MCV began overnight when a lower-tropospheric mesoscale vortex formed on the northern end of the north-south-oriented convective line. Intensification of the midtropospheric vortex followed, occurring in response to the development of a stratiform precipitation region" (Davis and Trier, 2002).

A number of these studies have indeed provided partial answers to the questions regarding the generation mechanism of absolute vorticity in the MCV. However, as Raymond and Jiang stated, "further work is needed in determining the contribution from each effect in a variety of mesoscale systems". The purpose of this paper is to take a more detailed look at the vorticity generation mechanisms, both in terms of PV and absolute vorticity.

In terms of the absolute vorticity budget, the primary intensification mechanism is by means of the thermally direct circulation driven by diabatic heating within the convective system and the associated flux convergence of planetary and relative vorticity. When referring more directly to potential vorticity (PV), the intensification can be explained (at least partially, when viewed in geometric coordinates, using the material form of the PV equation) in terms of the vertical gradient of diabatic heating within the convective system. In either case, diabatic heating is required, whether it be by driving the thermally direct circulation or producing PV by vertical gradients.

The aim of this paper is to resolve a number of ambiguous conclusions regarding the sources of PV in MCVs. In their satellite-based study of MCVs, Bartels and Maddox (1991) concluded that "the rapid mesovortex generation observed can be explained by the stretching term of the vorticity equation". This conclusion was limited to those MCVs for which a visually recognizable signature existed in satellite imagery – preferentially in weak shear. Seven years later, Weisman and Davis (1998) argued that

ACPD
9, 7531–7554, 2009

"for systems that develop in an environment with weak-to-moderate shear, a line-end vortex pair is generated primarily via the tilting of horizontal vorticity generated within the system-scale cold pool" and that "convergence at midlevels enhances Coriolis rotation over the longer term, leading to the preferred development of a cyclonic vortex". These ambiguities apply both to the budgets of absolute vertical vorticity as well as to respective roles of the convective and stratiform precipitation regions of MCSs. Regarding the former, for example, some studies have concluded that tilting of vorticity is the primary contributor to the formation of MCVs (Skamarock et al., 1994; Weisman and Davis, 1998), but others have found vortex tube stretching to be the primary vorticity generation mechanism at mid-levels (Brandes, 1990; Bartels and Maddox, 1991; Johnson and Bartels, 1992; Davis and Trier, 2002), and still others have suggested that both mechanisms may be important at different stages of the MCV life cycle (Cram et al., 2002) or at different scales of atmospheric motion (Knievel and Johnson, 2003). To resolve some of the uncertainty surrounding the relative contributions of tilting and stretching in the generation of cyclonic vorticity in MCVs, we will perform detailed analyses of the circulation budget of simulated MCVs over their lifetime, from genesis to maturity. Additionally, our idealized simulations will start with a basic state in thermal wind balance and include the effects of larger scale atmospheric systems, something which was not included in the Skamarock et al. (1994) and Weisman and Davis (1998) simulations.

As a part of this goal, we will also conduct a detailed look at the PV development process and the merger process of PV elements in order to make a cursory investigation into the role of PV generation on the storm scale (small, intense, convective updrafts) as well as on the MCV scale. Such a look is intended to reveal the role of vorticity on smaller scales, which is primarily generated by tilting mechanisms, on the development of vorticity at the larger, MCV scale as well as the flux convergence of planetary vorticity and relative vorticity on the system-wide scale. Given the linear hodographs employed in all basic states used to date in idealized studies of MCV dynamics, one would expect tilting to generate positive and negative relative vorticity centers in nearly

ACPD
9, 7531–7554, 2009

equal amounts (e.g. Rotunno, 1981). When tilting occurs in conjunction with a convective updraft, the vertical gradients of diabatic heating produce a concentration of PV substance (e.g. Tory et al., 2007) in mid-levels and a dilution of PV substance above, resulting in positive and negative PV anomalies, respectively. The evolution of these positive and negative PV centers can be monitored in numerical simulations to discover their relative contributions to the MCV PV.

It is consistently observed that the MCV resides in the stratiform precipitation region of MCSs. However, the magnitude of convective versus stratiform processes contributing to the PV generation in MCVs is less well understood. Many studies attribute the PV production to diabatic heating gradients that are present in the stratiform precipitation region of an MCS (Hertenstein and Schubert, 1991; Johnson and Bartels, 1992; Fritsch et al., 1994; Davis and Trier, 2002). This common belief is supported by the fact that MCVs are consistently observed to develop in the stratiform portion of MCSs. However, the diabatic heating profiles presented by Houze (1997, 2004) imply that the PV-generation may come from either convective or stratiform processes. It can be also argued, using a conceptual model of the MCS, such as presented in Fig. 14 of Houze (2004), with air ascending in convective elements at the leading edge of the MCS then moving rearward to the stratiform precipitation region, that the PV production by stratiform and convective processes might even be considered inseparable because both are part of the same process.

Indeed, deep convection often occupies a relatively small area (by percentage) of an MCS, but the diabatic heating rates and vertical mass flux per unit area are at least an order of magnitude greater, locally, in convective than in stratiform precipitation, making it unclear which is the bigger contributor to the PV and the absolute vorticity on a system-wide scale. Again, since most of the mass flux is processed through the leading convective region and the stratiform precipitation, it can be argued that both may be similar contributors. The present study will clarify this issue by performing a detailed analysis of the diabatic heating profiles. These diabatic heating profiles should reveal the quantity of mass processed through the convective system since diabatic

ACPD
9, 7531–7554, 2009

heating rate is proportional to the mass flux.

2 Simulations

The simulations were part of an investigation into the mechanisms for the development of MCVs in weak but non-trivial baroclinic environments by Conzemius et al. (2007) and are further described in that study. The goal of the original study was to conduct idealized simulations capable of coarsely resolving deep convective processes in an environment with relatively weak shear, whereby the dynamics of MCV maintenance and growth could be examined, but still encompassing an area large enough that permits larger scale baroclinic development as part of the MCV lifecycle.

For this study, we conducted two simulations, the primary difference between which was the value of ambient CAPE. The first simulation was designated the control simulation and started with a basic state thermodynamic profile that was neutral to the moist ascent of boundary layer air parcels. By definition, this neutral atmosphere had no CAPE, but CAPE developed during the simulation, reaching maximum values of around 700 $J\,kg^{-1}$. The second simulation had 2000 $J\,kg^{-1}$ CAPE in the center of the baroclinic zone and was simply designated as the CAPE simulation.

We performed both simulations using the MM5 model (Grell et al., 1994), which is a limited area, non-hydrostatic, sigma coordinate model. We performed the simulations on an 11 000 km by 5000 km domain using an outer, coarse-resolution grid with a 90 km grid interval and three nested inner grids whose intervals were 30, 10, and 3.3 km. The initial state consisted of an Eady-type baroclinic background, in which all variables are a function of latitude and pressure only. In order to initiate an MCS, we inserted a warm core, low-level vortex, with zero PV perturbation in its interior (to avoid preconditioning the simulation with interior PV) into the background state. The basic parameters of the simulations are listed in Table 1.

Conzemius et al. (2007) describe the evolution of these simulations in greater detail, so we will only summarize here. In the control simulation, an MCS developed approx-

ACPD
9, 7531–7554, 2009

imately 126 h into the simulation, within an intensifying, moist baroclinic cyclone. An MCV developed within the MCS, and the MCS precipitation gradually became more stratiform in nature as the simulation proceeded. In the CAPE simulation, the MCS developed approximately 150 h into the simulation (this was delayed due to the choice of an isolated initial vortex temperature radial profile), but when the growth occurred, it was much more rapid and extensive. The MCV that developed was much stronger as well, with the precipitation shield remaining convective much longer into the simulation.

3 Diagnostic calculations

3.1 Vorticity budget calculations

Similar to the procedure expounded in Haynes and McIntyre (1987) and the methodology outlined in Weisman and Davis (1998), Cram et al. (2002) and Davis and Trier (2002), we use the flux form of the vorticity equation and calculate area- and temporal-averages of the circulation tendency:

$$\frac{\partial \zeta_a}{\partial t} = -\frac{\partial}{\partial x}\left(u\zeta_a + \omega\frac{\partial v}{\partial p} - G\right) - \frac{\partial}{\partial y}\left(v\zeta_a - \omega\frac{\partial u}{\partial p} + F\right) \quad (1)$$

where ζ_a is the absolute vorticity defined as $\zeta_a = f + \partial v/\partial x - \partial u/\partial y$, and F and G represent the horizontal components of the effects of additional forces, such as friction, which are neglected in this analysis for simplicity. The neglect of frictional forces can be justified by the fact that the initial near-surface winds are very weak and is further supported by the comparisons between vorticity budget profiles and actual vorticity change presented in Sect. 4.1.

In addition to avoiding the inherent problem of measuring the small difference between large terms that can occur when using the material form of the vorticity equation (Haynes and McIntyre, 1987), the strength of this method lies in the fact that, through Gauss's theorem, the tendency of the circulation for any enclosed area fixed in space

ACPD
9, 7531–7554, 2009

can be written in terms of the line integral of the flux component normal to the boundary of the area (Davis and Trier, 2002):

$$\frac{\partial C}{\partial t} = \iint_A \frac{\partial \zeta_a}{\partial t} = -\oint \left(\boldsymbol{u}\zeta_a - \omega \hat{\boldsymbol{k}} \times \frac{\partial \boldsymbol{u}}{\partial p} \right) \times \hat{\boldsymbol{n}} dl \tag{2}$$

where C is the absolute circulation, A represents the area encompassed by the closed loop, and $\boldsymbol{u}$ the horizontal velocity. We will refer to the first term under the integral as the horizontal convergence of absolute vorticity (horizontal flux term). A comparison between the flux and the material forms of the vorticity equation reveals that the horizontal flux term in Eq. (2) is equivalent to the horizontal advection term plus the stretching term in the material form of the vorticity equation. The second term is an amalgamation of the vertical advection of vertical vorticity and the tilting of horizontal vorticity into vertical vorticity and will be hereafter denoted simply as the tilting-like term (see Tory et al., 2007 for clarification of this terminology). For comparison, Davis and Trier (2002) refer to these terms as stretching and tilting, respectively.

The corresponding form of the PV equation is most conveniently written in theta (potential temperature) coordinates:

$$\iint_A \frac{\partial (\sigma Q)}{\partial t} = -\oint \left(\boldsymbol{u}\sigma Q - \dot{\theta} \hat{\boldsymbol{k}} \times \frac{\partial \boldsymbol{u}}{\partial \theta} \right) \times \hat{\boldsymbol{n}} dl, \tag{3}$$

where Q is PV ($m^2\,s^1\,K\,kg^1$), σ the isentropic density ($m^{-2}\,K^{-1}\,kg$), and $\dot{\theta}$ the material rate of change of potential temperature. In theta coordinates, the PV substance σQ is simply $\partial v/\partial x - \partial u/\partial y + f$, so one can see a striking similarity between Eqs. (2 and 3) (the zonal and meridional partial derivatives of course being taken on surfaces of constant pressure and potential temperature, respectively). Tory et al. (2007) and Haynes and McIntyre (1987) discuss the PV equation at length, and in particular, the second term in the line integral can be split into two terms, one of which describes tilting-like effects and the other describing vertical advection-like effects. The tilting-like and vertical advection-like terms tend to largely balance each other, typically leaving

ACPD
9, 7531–7554, 2009

the first term in the line integral as the dominant term on the right hand side of Eq. (3). Thus, we would expect an increase in PV substance over any area to be mostly due to flux convergence (i.e. a concentration) of PV. This concentration of PV substance occurs mostly at low-levels, driven by diabatic heating within the MCS. At upper levels, we would expect a negative PV anomaly to form as flux divergence dilutes the PV substance.

3.2 Areas and times of analysis on innermost grid

The rectangle forming the contour of integration was chosen to be as close to the vortex center while encompassing all significant cyclonic relative vorticity. In practice, the southern line segment was placed along the maximum 850–700 mb rear inflow into the convective system, while the western and northern line segments were placed as close as possible to the cyclonic vorticity maximum but in regions encountering little or no convection. To allow for the movement of the convective system within the averaging time interval, we placed the eastern line segment far enough ahead of the convective line that the precipitation did not advance beyond the eastern line until after the end of the averaging time interval.

Four time periods, each of 288 min duration, were chosen for the vorticity budget analysis of the control simulation. The chosen time periods encompass 1. initiation and organization of deep convection accompanied by intensification of the baroclinic cyclone, 2. expansion of the stratiform precipitation region and slight weakening of convection (very little deepening occurs during this phase), 3. a period of essentially no deepening of the baroclinic cyclone, and 4. a later period, characterized by a resumption of deepening. The line integral was calculated at each model level on the innermost 3.3-km domain at 8 min intervals, and time averaging was performed over the 288-min analysis period.

For the CAPE simulation, the time averaging periods were 240 min each. The first period corresponds to the development and organization of the MCS and intensification of the baroclinic cyclone. The next two periods correspond to the continued expansion

ACPD
9, 7531–7554, 2009

of the stratiform precipitation area, during which time the baroclinic cyclone did not deepen (at least in terms of surface pressure) significantly. The final period saw a resumption of rapid deepening of the baroclinic cyclone.

3.3 Convective versus stratiform partitioning method

Since the potential vorticity time tendency is driven by the horizontal flux convergence of PV substance (Eq. 3), and the absolute vorticity tendency is also affected by horizontal flux convergence (Eq. 2), one can invoke mass conservation to relate the flux convergence of either quantity to the updraft mass flux within the MCS. By partitioning the updraft mass flux into a convective and a stratiform portion (based on updraft speed), one can assess the contributions of convective and stratiform areas to the concentration of absolute vorticity or PV within the system. If the horizontal flux of absolute vertical vorticity dominates the circulation tendency in Eq. (2), one can use the vertical mass flux to establish the relative importance of stratiform and convective mass flux to the spin-up of absolute vorticity. Since the vertical mass flux is directly related to the diabatic heating rate in the system (we assume that the diabatic heating rate is essentially balanced by the upward transport of smaller potential temperature), it is equally useful to use diabatic heating rate as a proxy for mass flux. Our initial calculations demonstrated that the mass flux profiles (not shown) were qualitatively very similar to the profiles of diabatic heating rate.

We partitioned the convective and non-convective areas on the finest scale grid according to the vertical velocity at 600 mb. If the absolute value of vertical velocity at 600 mb exceeded $1\,\mathrm{m\,s^{-1}}$, we assigned the entire grid column to the convective area. Where the absolute value of the vertical velocity was equal to or less than $1\,\mathrm{m\,s^{-1}}$, we made a further distinction to separate stratiform precipitation areas from non-precipitation areas (generally outside the MCV). We assigned the grid column to the stratiform area if the rain water content was greater than $10^{-16}\,\mathrm{g\,kg^{-1}}$ and assigned it to the non-precipitation bin if the rain water content was less than or equal to $10^{-16}\,\mathrm{g\,kg^{-1}}$.

ACPD
9, 7531–7554, 2009

4 Sources of absolute vorticity and PV

4.1 Vorticity budget profiles

For approximately ten hours after the initiation of deep convection in the control simulation (Fig. 1a, b), the tilting-like term is a contributor to the creation of positive vertical vorticity in the lower atmosphere, but its calculated contribution is very sensitive to small changes in the placement of the southern line segment of the rectangle. The tilting-like term becomes large only when the southern line segment intersects individual convective cells, which make strong contributions to the vorticity budget on scales smaller than the size of the MCS itself (Knievel and Johnson, 2003). Nevertheless, the tilting-like term is consistently a positive contributor to absolute vorticity in the lowest levels of the troposphere up to about 700 mb. On an MCS-wide scale, the horizontal flux is, by far, the dominant mechanism responsible for the spin up of mid-level cyclonic absolute vorticity. The horizontal flux in Fig. 1a and b is strongest at low levels, consistent with a divergence profile associated with convection (Houze, 1997).

By t=129.6 h (Fig. 1b), a closed circulation is evident at 700 mb (not shown). Between t=124.8 and t=134.4 h into the simulation, the mid-level circulation strengthens substantially. This pattern is consistent with the re-intensification of the 27–28 May 1998 MCV investigated by Davis and Trier (2002). The stratiform precipitation is also expanding rapidly, and during this time, the horizontal flux convergence of absolute vertical vorticity is reflective of the stratiform divergence profile suggested by Houze (1997), with its flux convergence maximum at higher altitude than in Fig. 1a. In the ensuing time period (Fig. 1c), the circulation tendency is strongly positive in the upper troposphere, due to the horizontal flux divergence of negative relative vorticity.

At a much later time (Fig. 1d), when the surface low undergoes a steadier strengthening, the circulation budget is almost entirely dominated by the horizontal flux term. The dominance of this term shows that the mean secondary circulation associated with the vortex (convergence at low levels, rising in the vicinity of the vortex, and divergence at upper levels) drives the strengthening of the circulation, but this result might also be

ACPD
9, 7531–7554, 2009

an artifact of the analysis area. Due to the size and orientation of the MCS, it was difficult to place the southern portion of the line integral along the maximum rear inflow into the system. The system is also much less convective at this time.

In the CAPE simulation (Fig. 2), the evolution of the vorticity budget is somewhat different. In the initial time period (Fig. 2a), the horizontal flux convergence term is responsible for all the spin-up of absolute vorticity below the 500 mb level, except for the lowest 100 mb (where cold pool effects occur – see below). Thereafter (Fig. 2b and c), the flux convergence term actually becomes a negative contributor to the absolute vorticity below about 600 mb, and the spin up of absolute vorticity is provided solely by the tilting-like term. It appears that the cold pool generation is influencing the flux convergence during this time as the plots of 1000 mb temperature show a significant cold anomaly (as much as 10°C) spreading radially outward. In mid levels, however, the flux convergence is a contributor to the intensification of cyclonic absolute vorticity. At the very end of the time period of analysis (Fig. 2d), the horizontal flux convergence again dominates the absolute vorticity budget. By this time, however, the area of integration is so large that the contribution from tilting processes (which themselves are strongly dominated by individual thunderstorm updrafts and downdrafts) become small relative to the vorticity over the large integration area, and individual cells, which cross the boundary and would contribute most strongly to the tilting part of the circulation budget, contribute less to the area-integrated vorticity.

4.2 Stratiform and convective contributions to vortex intensification

A time sequence of plots of the convective and stratiform areas (not shown) in the control simulation reveals that the convection, as defined in Sect. 3.3, never occupies more than two percent of the area of analysis and never more than 12.5 percent of the total precipitation area, which reaches 53 000 km^2. Within a few hours of the initial convective development (t=124.8 to t=129.6 h), the stratiform region begins to expand rapidly. During the latter stages of expansion, the total area covered by convection decreases 65 percent from its maximum, and eventually, stratiform precipitation accounts

ACPD
9, 7531–7554, 2009

for 99 percent of the total precipitation area.

In the CAPE case, the precipitation area is considerably larger, reaching a maximum of 400 000 km^2. The convection occupies a maximum of 38% of the total precipitation area at t=153 h and reaches a maximum area over 15 000 km^2 at t=156 h. After that point, the convective area very slowly decreases while the stratiform and total precipitation areas rapidly expand, so that the convective area is roughly half its maximum size by the end of the simulation, and it occupies only two percent of the precipitation area. The convection provides a much greater contribution to the MCV diabatic heating and mass flux in the CAPE case.

Animations of relative vorticity (not shown) suggest the dominance of tilting at smaller scales (e.g. Knievel and Johnson, 2003), but on an MCV-wide scale, the horizontal flux convergence is, by far, the dominant contributor to vertical vorticity.

The evolution of the diabatic heating profiles in both the control and CAPE simulations is reflective of the evolution of the MCS (see Fig. 3). In the initial time period (Fig. 3a), the convection develops very rapidly, and convection dominates the diabatic heating. This fact alone strongly suggests that the deep convection is primarily responsible for the initial, rapid development of the MCV. By t=134.4 h (Fig. 3b), the stratiform precipitation region has expanded to occupy 50 percent of the area of the analysis, and this expansion is reflected in the diabatic heating profiles. The stratiform profile is qualitatively consistent with the stratiform diabatic heating profile shown in Fig. 3c of Houze (1997), further indicating an increasing contribution of stratiform precipitation to the vortex intensification. However, the diabatic heating is, overall, relatively weak in Fig. 3b, a feature that is consistent with the fact that, during this particular time interval, the vortex does not intensify significantly.

During the final time period (Fig. 3c), as the system reaches a regime of steady intensification, the diabatic heating increases, and most of this diabatic heating (and therefore the PV generation) is accomplished by the stratiform precipitation areas within the system. By this point, the diabatic heating probably reflects the moist baroclinic intensification at least as much as it is a sign of MCV dynamics. Indeed, Conzemius et

ACPD
9, 7531–7554, 2009

al. (2007) show that, during this stage of intensification, the conversion of mean state available potential energy (APE) to eddy APE increases in tandem with the diabatic production of eddy APE. Nevertheless, the MCS dynamics are a contributor to this process by providing diabatic support to the baroclinic cyclone intensification, and balanced MCV dynamics play a part in the maintenance of convection (Conzemius et al., 2007; Trier and Davis, 2002). It is noteworthy that, during this final period, the vertical gradients in diabatic heating are largest in the lower troposphere (much like the convective profile is, see Houze, 2004), yet the precipitation is 99% stratiform. This characteristic is symptomatic of the fact that the system lacks substantial deep convection, has grown upscale, and therefore no longer resembles an MCS. It lacks a mid-level layer of dry air (through which falling precipitation might bring about a net cooling) that would be characteristic of compensating downdrafts in the vicinity of convective updrafts. The only cooling occurs below about 900 mb.

Overall, the results indicate a system in which convective contributions to PV are relatively large at first but acquiesce to stratiform contributions as the stratiform precipitation area expands (Cram et al., 2002).

In the CAPE simulation (Fig. 3d through f), the diabatic heating profile undergoes a somewhat similar evolution as in the control simulation, but unlike the control simulation, the convection accomplishes most of the diabatic heating throughout the analysis period. At first (Fig. 3d), there is a very strong convective area contribution to the diabatic heating profile. As the stratiform area rapidly expands (Fig. 3e), its contribution to the total becomes more significant, but its sign is also opposite that of the convective profile. It is clear that the deep convection accomplishes the bulk of the flux convergence of PV substance (see Eq. 3); the vertical gradient of diabatic heating in the stratiform profile does not indicate a significant PV vertical advection-like effect (Tory et al., 2007). In the final period (Fig. 3f), the stratiform diabatic heating profile becomes more consistent with the idealized profile shown in Houze (1997) and is more favorable for contributing to PV in the mid-troposphere. Still, the convective contribution is larger. Overall, Fig. 3 shows that the stratiform areas had little contribution to the PV

ACPD
9, 7531–7554, 2009

production in the CAPE simulation.

Given our definitions of stratiform and convective precipitation areas employed in this analysis, it certainly appears from Fig. 3 that the stratiform areas of the MCS are not the major PV producers in the CAPE simulation. Although relatively shallow areas of positive vertical gradients of diabatic heating exist, most of these positive vertical gradients are found in the convective regions. This is not to say that one 3 km simulation provides undisputable proof that the PV production occurs only in convective updrafts of an MCS. In fact, the 3 km resolution is relatively coarse for resolving processes essential to individual convective updrafts (e.g. Bryan et al., 2003). However, we contend that the simulation performs reasonably well at resolving processes on the scale of the MCS, and the results are believed usefully suggestive of the fact that much of the PV production is accomplished by deep convection.

4.3 Illustration of the PV evolution

In order to further illustrate this evolution as well as the importance of convective processes to the generation of PV, we show PV horizontal cross sections at 700 mb (Fig. 4), which are taken from PV animations that were constructed from the MM5 output on the innermost (highest resolution) domain. The animation shows the creation of strong, small scale positive and negative PV anomalies that are associated with individual thunderstorm updrafts whose vorticity has opposite signs due to tilting (Cram et al., 2002). At t=156.7 h (Fig. 4a), three positive PV anomalies, labeled "A", "B", and "C", are shown. By t=158.3 h (Fig. 4b), as the convection expands outward, these three centers move rearward relative to the convection and begin to rotate cyclonically about a common center. Center A has moved very slightly to the west, B has moved north, and C has moved most rapidly northeast. At t=160.0 h (Fig. 4c) the PV centers have rotated about the center of the MCV, and by t=161.7 h (Fig. 4d), the PV anomaly B has moved very close to the center of the MCV. All three anomalies are rotating in a cyclonic fashion about this center. This rotation comes about due to the flux convergence of planetary vorticity as the system rapidly intensifies due to the diabatic heating. One

ACPD
9, 7531–7554, 2009

would also note in the simulations an association with the rear inflow jet and perhaps a tilting contribution as the rear inflow jet descends, but the analyses above indicate the large scale flux convergence of absolute vorticity on the system scale as the primary source of the vorticity. In all frames, intense PV centers are created by the leading edge convection, then move rearward and become somewhat less intense. The positive centers are sufficiently dominant such that, once they have moved rearward to the stratiform area, a combination of numerical diffusion, and quite possibly some degree of PV merger processes as well (although the processes do appear mostly diffusive in the animation) smoothes the anomalies, and only weaker positive PV anomalies remain.

5 Conclusions

The purpose of this study was to examine the vorticity budgets and diabatic heating profiles of the simulated system to ascertain the sources of vorticity generation as well as quantify the contributions of convective and stratiform precipitation areas to the budgets and profiles. We analyzed two simulations here. In the first simulation (control), the MCS developed in a region of approximately 600–700 $\mathrm{J\,kg^{-1}}$ CAPE in an otherwise moist neutral environment. The second simulation had a background state of considerably larger CAPE, reaching 3000 $\mathrm{J\,kg^{-1}}$.

There are two findings common to both simulations. First, the creation of the initial, lower tropospheric cyclonic PV anomaly is the result of diabatic processes most active in the deep convective region of the MCS. Convection may play the leading role in the creation of at least the initial PV anomaly complex. Second, the cyclonic absolute vorticity anomaly stems primarily from the flux convergence of absolute vorticity due to the diabatic heating within the convective system. Tilting appears to be important only at the scale of individual convective updrafts and, in fact, produces vorticity centers of opposite sign.

Some significant difference between the control and CAPE simulations exist as well,

ACPD
9, 7531–7554, 2009

and these differences are consistent with the differences in the background convective instability and the moisture available for diabatic processes within the convective systems. In the control simulation, convection is initially the primary driver of the diabatic heating that is responsible for the cyclonic PV generation. When the MCV has become established, the convection diminishes, and the stratiform precipitation area expands, making the stratiform precipitation the dominant contributor to PV production. However, in the higher CAPE simulation, the majority of PV production was in the convective regions during the entire period of analysis. In other words, the stratiform precipitation became increasingly important in the control simulation, but this importance was realized only after most of the convection had ceased. In the CAPE simulation, the PV evolution can be explained by intense production associated with the convection at the leading edge of the MCS, followed by reorganization and distribution of the PV in the stratiform region. Indeed, the animations of PV show that intense production occurs in the leading edge where convection is active, and the corresponding PV then moves rearward into the stratiform precipitation region where the MCV resides. The results are at least suggestive of the possibility that most of the flux convergence of absolute vorticity, as well as the PV production in MCVs, occurs in the convective region of MCSs, provided convection is active. This conclusion, while very plausible based on the evidence presented herein, requires a more comprehensive sampling of the observed lifecyle of MCVs. The BAMEX data set appears ideally suited for this purpose.

Acknowledgements. This work was conducted under the support of NSF grant ATM-0305412 and the U.S. Naval Postgraduate School in Monterey, California, USA.

References

Bartels, D. L. and Maddox, R. A.: Midlevel cyclonic vortices generated by mesoscale convective systems, Mon. Weather Rev., 119, 104–118, 1991.

Brandes, E. A.: Evolution and structure of the 6–7 May 1985 mesoscale convective system and associated vortex, Mon. Weather Rev., 118, 109–127, 1990.

Bryan, G. H., Wyngaard, J. C., and Fritsch, J. M.: Resolution requirements for the simulation of deep moist convection, Mon. Weather Rev., 131, 2394–2416, 2003.
Conzemius, R. J., Moore, R. W., Montgomery, M. T., and Davis, C. A.: Mesoscale convective vortex formation in a weakly sheared moist neutral environment, J. Atmos. Sci., 64, 1443–1466, 2007.
Cram, T. A., Montgomery, M. T., and Hertenstein, R. F. A.: Early evolution of vertical vorticity in a numerically simulated idealized convective line, J. Atmos. Sci., 59, 2113–2127, 2002.
Davis, C. A. and Trier, S. B.: Cloud-resolving simulations of mesoscale vortex intensification and its effect on a serial mesoscale convective system, Mon. Weather Rev., 130, 2839–2858, 2002.
Fritsch, J. M., Murphy, J. D., and Kain, J. S.: Warm core vortex amplification over land, J. Atmos. Sci., 51, 1780–1807, 1994.
Grell, G. A., Dudhia, J., and Stauffer, D. R.: A description of the fifth-generation Penn State/NCAR mesoscale model (MM5), NCAR Tech. Note NCAR/TN-398_STR, 117 pp., 1994.
Haynes, P. H. and McIntyre, M. E.: On the evolution of vorticity and potential vorticity in the presence of diabatic heating and frictional or other forces, J. Atmos. Sci., 44, 828–841, 1987.
Hertenstein, R. F. A. and Schubert, W. H.: Potential vorticity anomalies associated with squall lines, Mon. Weather Rev., 119, 1663–1672, 1991.
Houze Jr., R. A.: Stratiform precipitation in regions of convection: A meteorological paradox?, B. Am. Meteorol. Soc., 78, 2179–2196, 1997.
Houze Jr., R. A.: Mesoscale convective systems, Rev. Geophys., 42, RG4003, doi:10.1029/2004RG000150, 2004.
Johnson, R. H. and Bartels, D. L.: Circulations associated with a mature-to-decaying midlatitude mesoscale convective system. Part II: upper-level features, Mon. Weather Rev., 120, 1301–1321, 1992.
Knievel, J. C. and Johnson, R. H.: A scale-discriminating vorticity budget for a mesoscale vortex in a midlatitude, continental mesoscale convective system, J. Atmos. Sci., 60, 781–794, 2003.
Raymond, D. J. and Jiang, H.: A theory for long-lived mesoscale convective systems, J. Atmos. Sci., 47, 3067–3077, 1990.
Rotunno, R.: On the evolution of thunderstorm rotation, Mon. Weather Rev., 109, 577–586,

ACPD
9, 7531–7554, 2009

1981.
Skamarock, W. C., Weisman, M. L., and Klemp, J. B.: Three-dimensional evolution of simulated long-lived squall lines, J. Atmos. Sci., 51, 2563–2584, 1994.
Tory, K. J., Montgomery, M. T., Davidson, N. E., and Kepert, J. D.: Prediction and diagnosis of tropical cyclone formation in an NWP system. Part II: a diagnosis of tropical cyclone Chris formation, J. Atmos. Sci., 63, 3091–3113, 2007.
Trier, S. B. and Davis, C. A.: Influence of balanced motions on heavy precipitation within a long-lived convectively generated vortex, Mon. Weather Rev., 130, 877–899, 2002.
Weisman, M. L. and Davis, C. A.: Mechanisms for the generation of mesoscale vortices within quasi-linear convective systems, J. Atmos. Sci., 55, 2603–2622, 1998.

ACPD
9, 7531–7554, 2009

Table 1. Selected parameters for simulations.

			Control	CAPE
Basic State	T_{cent} (K)		293	303
	$Shear_{cent}$ ($m\,s^{-1}\,km^{-1}$)		1.5	1.5
	$Width_{BZ}$ (degrees)		60	60
	$CAPE_{cent}$ ($J\,kg^{-1}$)		0	2247
	$CAPE_{max}$ ($J\,kg^{-1}$)		0	4200
Inner domains	Start time (hours)		120	120
	Move frequency (hours)	D3	–	72
		D4	24	8
	Grid dimensions	D2	94×76	154×94
		D3	229×172	289×199
		D4	271×211	289×253
Initial vortex radial profile			Guassian	Isolated

ACPD
9, 7531–7554, 2009

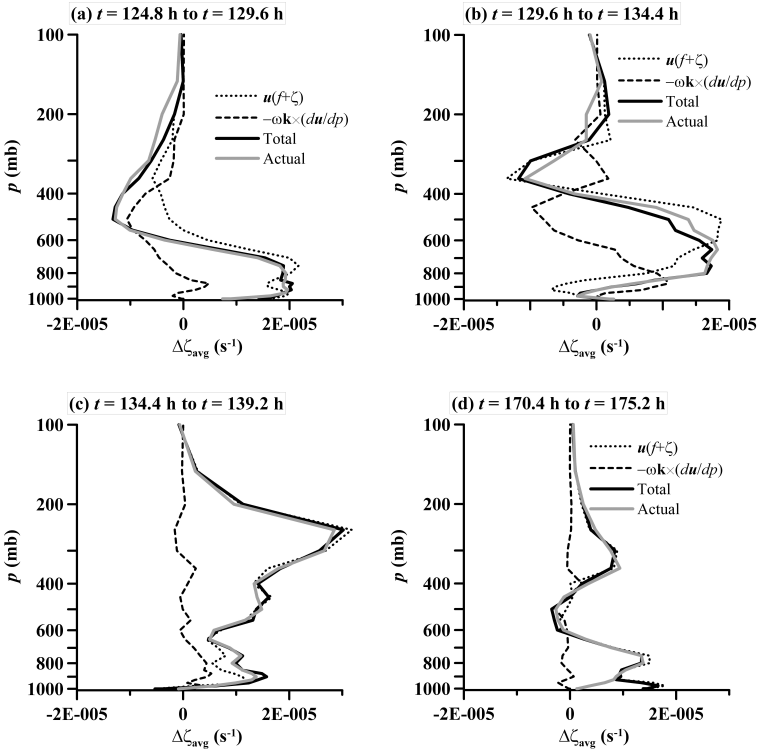

Fig. 1. Circulation budget analysis for a box surrounding the vortex in the control simulation on the 3.3-km grid for the time periods: **(a)** 124.8 h to 129.6 h; **(b)** 129.6 h to 134.4 h; **(c)** 134.4 h to 139.2 h; and **(d)** 170.4 h to 175.2 h, respectively. The dotted line indicates the horizontal flux convergence of absolute vorticity; the dashed line is the vertical flux term; the solid black line is the total of the horizontal and vertical terms; and the solid gray line is the actual change over the period of integration.

ACPD
9, 7531–7554, 2009

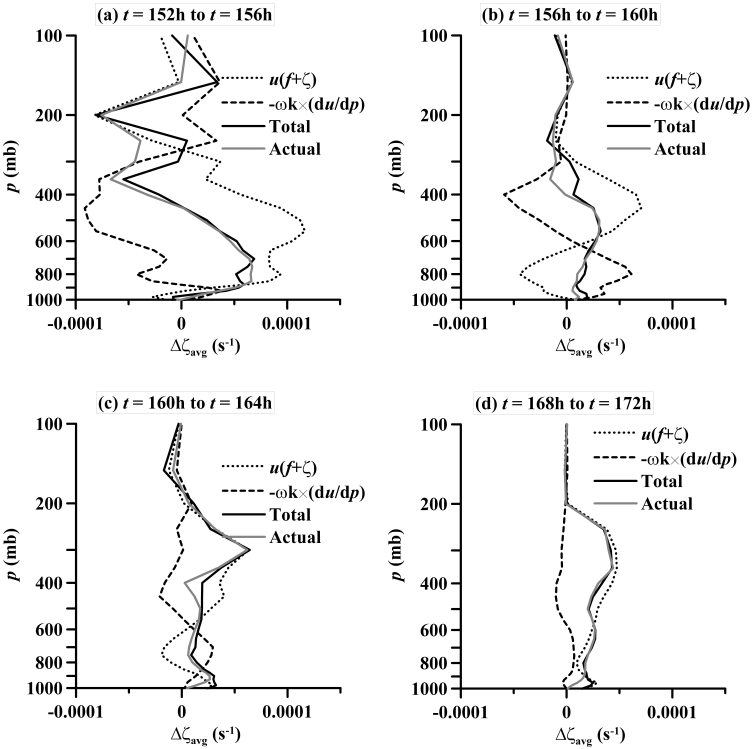

Fig. 2. Circulation budget analysis for the CAPE simulation for a box surrounding the vortex in the control simulation on the 3.3-km grid for the time periods: **(a)** 152 h to 156 h; **(b)** 156 h to 160 h; **(c)** 160 h to 164 h; and **(d)** 168 h to 172 h, respectively. For notation see Fig. 1.

ACPD
9, 7531–7554, 2009

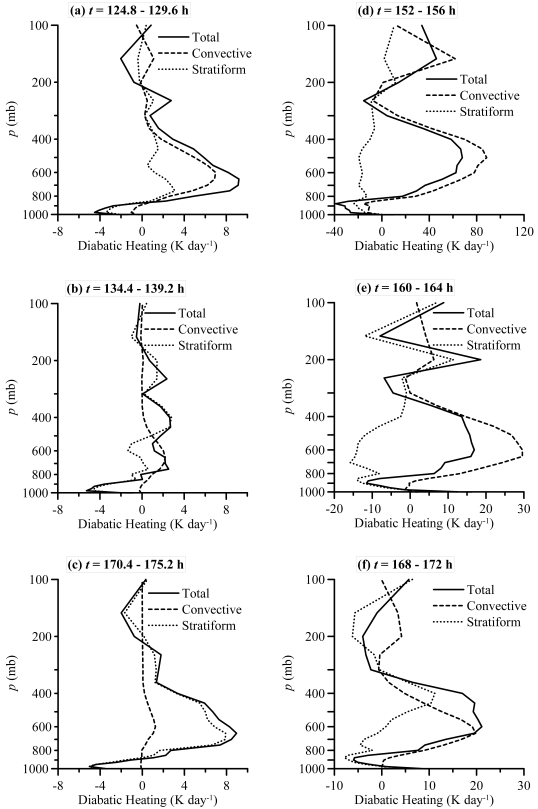

Fig. 3. Area-averaged diabatic heating, showing contributions from convective and stratiform precipitation regions in the control simulation, for a box surrounding the vortex on the 3.3-km grid, at simulation time: **(a)** 124.8 h to 129.6 h; **(b)** 134.4 h to 139.2 h; and **(c)** 170.4 h to 175.2 h, and for the CAPE simulation at **(d)** 152 h to 156 h; **(e)** 160 h to 164 h; and **(f)** 168 h to 172 h. The area average heating rate pertains to the analysis box, which is centered on the area of the circulation and has its southern edge roughly along the line of maximum rear inflow into the system.

ACPD
9, 7531–7554, 2009

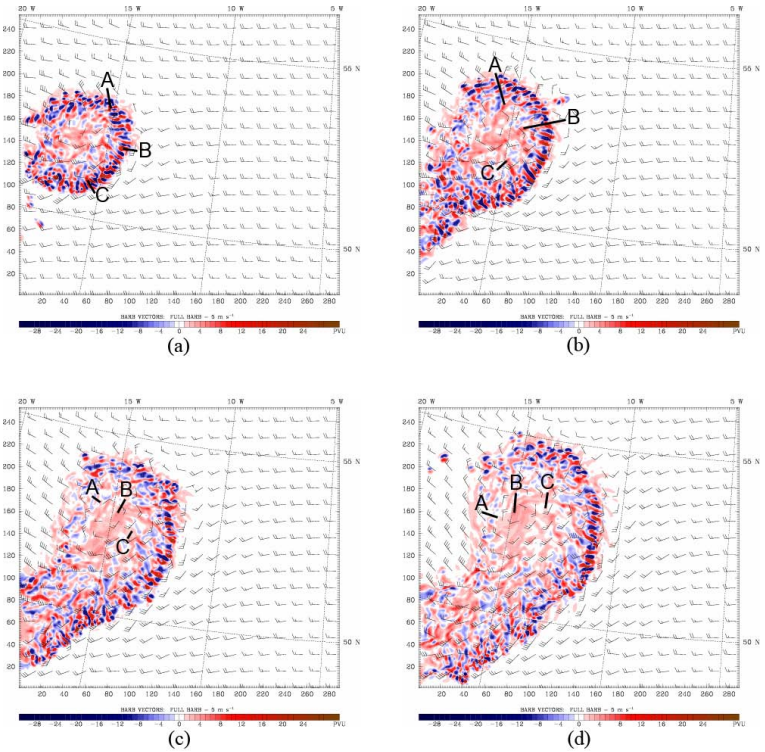

Fig. 4. Evolution of the PV (PVU) and winds (kt) on the 3 km domain of the MM5 CAPE simulation at the following times during the simulation: **(a)** 156.7 h; **(b)** 158.3 h; **(c)** 160.0 h; and **(d)** 161.7 h. The markings "A", "B", and "C" refer to three individual PV centers diagnosed at t=156.7 h into the simulation.

ACPD
9, 7531–7554, 2009